The general formulation of the energy equation and the impact of enthalpy diffusion on multi-component droplet heat and mass transfer

Artur Carvalho Santos[a,*], Fernando Luiz Sacomano Filho[b], Aymeric Vié[a,c]

[a] *Laboratoire EM2C, CNRS, CentraleSupélec, Université Paris-Saclay, Gif-sur-Yvette, France.*

[b] *Laboratory of Environmental and Thermal Engineering, Universidade de São Paulo, São Paulo, Brazil.*

[c] *Fédération de Mathématiques, CentraleSupélec, Université Paris-Saclay, Gif-sur-Yvette, France.*

Abstract

A key aspect of modeling the heat and mass transport of droplets is the description of diffusion transport, and multiple approaches exist to address it. While many contributions focus on the description of the mass transfer, details about the energy formulation to describe the droplet's heat transfer are seldom developed in the literature. This work demonstrates that a general gas-phase energy formulation can be obtained independently from the species diffusion transport modeling while incorporating multi-species enthalpy diffusion terms with a simple expression. Considering the ideal gas simplification, it is shown that a simple choice of specific heats is sufficient to characterize the inclusion or not of multi-species enthalpy diffusion effects. Furthermore, it is also demonstrated that the final energy expression degenerates in the single-component limit to the same energy formulation as in the model of (Abramzon and Sirignano, Int. J. Heat and Mass Trans, Vol.32(9), pp.1605-1618, 1989), considered as a reference in the literature. Simulations are conducted for droplets of multiple fuel compositions in varied atmospheric conditions to represent spray combustion scenarios and evaluate the impact of incorporating or not the enthalpy diffusion term, and conclude on the need and ease of use of the proposed energy formulation.

Keywords: Droplet evaporation, Multi-component droplets, Droplet heat transfer, Evaporation modeling, Spray combustion

*Corresponding author

Email address: artur.carvalho-santos@centralesupelec.fr (Artur Carvalho Santos)

1. Introduction

To characterize droplet phase-change mechanisms in spray configurations, fuels are often described using single-component models [1] based on a surrogate representation of the fuel. However, realistic liquid mixtures are composed of a significant number of species, making the use of multi-component models necessary. Further, for general applications, the effect of non-ideal mixtures should also be incorporated into the modeling strategy. Non-ideality can be present for many mixtures, for instance, biofuels, e.g., hydrophilic fuels such as alcohols in the presence of water [2], [3]. Even conventional fuels, e.g., aeronautical kerosene, may require more complex modeling, since hydrocarbons with ramified chains are often present [4], potentially raising non-ideal effects.

To take into account relevant non-ideal contributions, phase-change for groups of fuels must be described separately, and a primary requirement for this is the computation of mass transfer rates for each representative species. In this way, one additional challenge lies within the mass diffusion transport, specifically how to model diffusion velocities in a non-binary case [5], [6]. To tackle these issues, discrete component models (DCMs) [7] characterize the fuel using a reduced set of species representing the entire mixture's main physics. By employing this type of modeling strategy, mass transfer rates can be computed for each of the relevant species, instead of a single, global mass transfer rate. Still, the mass diffusion transport must be adressed. One possibility is to suppose that all species have the same average diffusion coefficient $\bar{D}$ in the gas phase, as done, for instance by Law et al. [2], [8]. However, this simple solution has the drawback of missing differential diffusion effects, thus overlooking the complexity of multi-component phase change and therefore the main advantage of a DCM. A possible improvement is allowing each species to have its diffusion coefficient [9, 10, 11, 3]. Different frameworks have been used to compute this diffusion coefficient, for instance, Blanc's model [12], Wilke's model [13], or the Hirschfelder-Curtiss formulation [14]. With such strategies, the species conservation equations can still be analytically integrated to account for multi-component phase-change effects without additional complexity compared to the single-component case.

Still, current DCMs have been proposed not only with these different mass diffusion coefficient closures but also using different energy formulations that are not always comprehensively detailed. Energy results are used mainly to predict the evolution of the droplet's temperature and heat transfer rates between itself and the gaseous phase, which can be of great importance. Even though the energy formulation is derived independently from the mass transfer developments, the influence of the diffusion velocities still appears explicitly in the enthalpy diffusion flux term. This creates an impact in the energy results from choices made for the mass transport modeling, which have already been shown to be potentially significant [15].

One hypothesis often used to develop the energy formulation is that specific heats are equal for all species in the gaseous phase. This manuscript shows that this can be equivalent to neglecting the enthalpy diffusion term. Therefore, the assumption of equal specific heats can be effectively seen as a simplifying approach that avoids having to describe the enthalpy diffusion term altogether. A second possibility can be

found in the droplet energy transfer models of Zhang and Kong [10], Grosshans et al. [16], Mahiques et al. [17], and Shen et al. [18], which were formulated by incorporating only conducto-convective effects through average heat transfer coefficients from classical boundary layer theory. However, when following this approach, the enthalpy diffusion and contributions from the Stefan flow generated from phase-change itself are neglected. As detailed in several references, e.g., [19],[20], Stefan flow effects can be paramount and should be incorporated into droplet phase-change models.

To include enthalpy diffusion effects, different strategies have been proposed by the literature. For instance, Lupo and Duwig [15] developed an analytical model following specific droplet phase-change hypotheses. For their energy formulation, the computation of a modified Spalding heat transfer number is proposed through a mathematical construct used to compute a quadrature at each time step involving differences between the average specific heats among fuel vapors and average specific heats among inert gases. Similarly, the energy formulation of Ebrahimian and Habchi [9] also proposes the introduction of a mathematical construct; in analogy with the binary case, a conversion between molar fraction gradients to mass fraction gradients is performed, allowing for the use of a correction velocity that ensures mass conservation. These remarks concerning the model of Ebrahimian and Habchi [9] also apply to others that follow the same general structure, e.g., the works of Long et al. [21] and Yi et al. [22]. Through these mathematical constructs, the approaches of Lupo and Duwig [15] as well as of Ebrahimian and Habchi [9] introduce functional dependencies into the energy equation developments.

In this way, the first objective of this work is to demonstrate, through the analytical derivation procedure, that enthalpy diffusion effects can be rigorously taken into account without needing more complex mathematical features. It is also demonstrated that the mass diffusion velocities closure should have no functional influence on the energy counterpart. Therefore, the proposed energy formulation is shown to be general concerning these choices while still applying to convective environments and rigorously incorporating Stefan flow effects. Furthermore, an additional contribution is that, in the single-component limit, the proposed formulation degenerates to the validated energy formulation proposed by Abramzon and Sirignano [23], and can therefore be regarded as a suitable extension of that model toward a general multi-component scenario. It is also shown that enthalpy diffusion effects can be impactful for droplet phase-change modeling, particularly in high-temperature scenarios and when surrounding conditions vary during the droplet's lifetime, justifying the importance of the proposed developments. To compute numerical results, our validated modeling strategy for the mass transfer proposed in [3] is used in this work; a summary of its characteristics is also provided here. The impact of considering or not enthalpy diffusion is then assessed for various liquid mixtures and environments representative of general applications.

The paper is organized as follows. First, the general equations and preliminary integrations are presented along with simplifying assumptions. Then, the detailed developments of the energy equation are presented, highlighting different options and the respective consequences on the final model. Details are also given on the species integration and the used numerical procedure. It should be noted that all of this work's

developments are carried out for spherical droplets and therefore do not directly apply to sessile droplets or other general shapes. Still, there is no theoretical barrier to deter the extension of the proposed results toward more general droplet shapes, which have been the focus of some recent publications specifically for spheroidal and sessile droplets [24], [25], [26]. Finally, numerical simulations are performed on cases of varying complexity to show the impact of the energy formulation, with a particular focus on including the enthalpy diffusion term through different expressions of specific heats. The paper ends with a summary of the main conclusions and perspectives.

2. Conservation equations and preliminary integrations

The gas-phase conservation equations for mass, species, and energy can be written as follows [5, 6, 27]:

$$\frac{\partial \rho}{\partial t} + \nabla \cdot [\rho \mathbf{u}] = 0, \tag{1}$$

$$\frac{\partial \rho Y_i}{\partial t} + \nabla \cdot [\rho Y_i \mathbf{v}_i^m] = \dot{\omega}_i, \tag{2}$$

$$\begin{aligned} \frac{\partial \rho h_s}{\partial t} + \nabla \cdot \left[\rho \left(\mathbf{u} h_s + \sum_{k=1}^{N} Y_k \mathbf{v}_k^D h_{s,k} \right) \right] = \frac{D\mathbf{p}}{Dt} + \boldsymbol{\tau} : \nabla \mathbf{u} + \nabla \cdot \boldsymbol{q}_R + \\ + \rho \sum_{k=1}^{N} Y_k \mathbf{v}_k^D \boldsymbol{f}_k + \nabla \cdot \left[RT \sum_{j=1}^{N} \sum_{k=1}^{N} \left(\frac{X_k D_j^T}{W_j \tilde{D}_{j,k}} \right) \left(\mathbf{v}_j^D - \mathbf{v}_k^D \right) \right] + \\ + \nabla \cdot [\lambda \nabla T] + \dot{\omega}_c, \end{aligned} \tag{3}$$

where ρ is the density, $\mathbf{u}$ the velocity, Y_i the mass fraction, $\mathbf{v}_i^m$ the average molecular velocity, $\dot{\omega}_i$ the species source term for chemical reactions, h_s the sensible enthalpy, $\mathbf{v}_i^D = \mathbf{v}_i^m - \mathbf{u}$ the mass diffusion velocity, $\mathbf{p}$ the pressure, $\boldsymbol{\tau}$ the viscous tensor, λ the thermal conductivity, T the temperature, $\boldsymbol{f}_i$ the volumetric forces, R the universal gas constant, X_i the molar fraction, $D_{j,k}^T$ the thermal diffusion coefficient, W_i the molecular weight, $\tilde{D}_{i,k}$ the binary diffusion coefficient in a multi-component mixture, $\boldsymbol{q}_R$ the radiative flux and $\dot{\omega}_c$ the energy source term due to chemical reactions. Subscripts i, j, k identify specific species.

The following assumptions for the gas phase are made:

1. Quasi-steadiness i.e $\partial/\partial t = 0$;
2. Spherical symmetry i.e. $\nabla \cdot \boldsymbol{\gamma} = \frac{d}{dr}[r^2 \boldsymbol{\gamma}]$ for any $\boldsymbol{\gamma}$ (only the radial dimension r is retained);
3. No chemical reaction i.e. $\dot{\omega}_k = 0 \ \forall k$, $\dot{\omega}_c = 0$;
4. Low-Mach, dilatable flow i.e. $\boldsymbol{\tau} = 0$, $\nabla \mathbf{p}$=0;
5. Negligible volumetric forces i.e. $\boldsymbol{f}_k = 0, \ \forall k$;
6. Negligible Dufour effects, i.e.:
   $\sum_{j=1}^{N} \sum_{k=1}^{N} \left(\frac{X_k D_j^T}{W_j \tilde{D}_{j,k}} \right) \left(\mathbf{v}_j^D - \mathbf{v}_k^D \right) = 0$;
7. Negligible radiation effects, i.e. $\boldsymbol{q}_R = 0$.

This allows us to simplify Eqs. 1,2,3, respectively into:

$$\frac{d}{dr}\left[r^2\rho\mathrm{u}\right] = 0, \tag{4}$$

$$\frac{d}{dr}\left[r^2\rho Y_i \mathrm{v}_i^m\right] = 0, \tag{5}$$

$$\frac{d}{dr}\left[r^2\rho\left(\mathrm{u}h_s + \sum_{k=1}^{N} Y_k \mathrm{v}_k^D h_{s,k}\right)\right] = \frac{d}{dr}\left[r^2\lambda\frac{dT}{dr}\right]. \tag{6}$$

The term $\sum_{k=1}^{N} Y_k \mathrm{v}_k^D h_{s,k}$ in Eq. 6 represents the enthalpy diffusion flux.

Integration of Eq. 4 over the spatial coordinate r leads to the result that defines the Stefan flow, which relates the advective velocity u to the droplet's global mass transfer rate $\dot{m}$:

$$\dot{m} = 4\pi r^2 \rho \mathrm{u}. \tag{7}$$

Similarly, integrating the simplified species conservation Eq. 5 over the spatial coordinate r yields:

$$\dot{m}_i = 4\pi r^2 \rho Y_i \mathrm{v}_i^m. \tag{8}$$

Opening up the molecular velocity as $\mathrm{v}_i^m = \mathrm{u} + \mathrm{v}_i^D$ while using the result of the integration of global mass conservation Eq. 7 to substitute for the advective velocity u leads to:

$$\dot{m}_i - \dot{m}Y_i = 4\pi r^2 \rho Y_i \mathrm{v}_i^D. \tag{9}$$

3. Energy integration

Using the same set of hypotheses as in Sec. 2, an analogous integration procedure is carried out for the energy. Integrating the simplified energy conservation Eq. 6 over the spatial coordinate r and using Eq. 7 leads to:

$$\dot{m}h_s + 4\pi r^2 \rho \sum_{k=1}^{N} Y_k \mathrm{v}_k^D h_{s,k} - 4\pi r^2 \lambda \frac{dT}{dr} = \dot{Q}, \tag{10}$$

where $\dot{Q}$ is the heat transfer rate reaching the surface of the droplet. The middle term in the LHS can be recast as:

$$\dot{m}h_s + \sum_{k=1}^{N} \left[4\pi r^2 \rho Y_k \mathrm{v}_k^D\right] h_{s,k} - 4\pi r^2 \lambda \frac{dT}{dr} = \dot{Q}, \tag{11}$$

Performing the substitution of Eq. 9 into Eq. 11 leads to:

$$\dot{m}h_s + \sum_{k=1}^{N} \left[\left(\dot{m}_k - \dot{m}Y_k\right) h_{s,k}\right] - 4\pi r^2 \lambda \frac{dT}{dr} = \dot{Q}. \tag{12}$$

The summation term in the LHS can be split, and the whole equation rearranged as:

$$\dot{m}\left[h_s - \left(\sum_{k=1}^{N} Y_k h_{s,k}\right)\right] + \sum_{k=1}^{N} \dot{m}_k h_{s,k} - 4\pi r^2 \lambda \frac{dT}{dr} = \dot{Q}, \tag{13}$$

The sensible enthalpy for the whole gaseous mixture can then be written as the sum of its components, i.e. $h_s = \sum_{k=1}^{N} Y_k h_{s,k}$, canceling out the first term in the LHS and yielding:

$$\sum_{k=1}^{N} \dot{m}_k h_{s,k} - 4\pi r^2 \lambda \frac{dT}{dr} = \dot{Q}. \tag{14}$$

Equation 14 is a general energy formulation for multi-component droplets with respect to the mass diffusion closure, provided that hypotheses #1-#7 of the previous section are made, which are customary for most models in the literature. It states that the heat transfer rate reaching the droplet's surface equals the difference between the enthalpy diffusive fluxes and the heat conduction in the gaseous phase.

A second analytical integration usually follows to be consistent with typical film theory treatments used to incorporate convection effects and avoid spatial discretizations. The following supplementary hypotheses must then be made:

8. Ideal gases i.e. $dh_{s,k} = c_{p,k} dT$;
9. Constant properties c_p, λ in space.

In CFD codes, the results from the second spatial integration are usually computed once for each time step, with properties also assumed to be constant within. Therefore, for most CFD codes, the assumption of constant properties during time steps is reasonable, as argued by Sazhin [1]. To average the properties in space, the so-called "one-third rule" [28],[29],[23] is here employed, as customary in the literature.

With these additional assumptions, Eq. 14 then becomes:

$$\sum_{k=1}^{N} \dot{m}_k c_{p,k} (T - T^s) - 4\pi r^2 \lambda \frac{dT}{dr} = \dot{Q}. \tag{15}$$

Eq. 15 above is then integrated by separation of variables from the surface of the droplet $r = R_d$ where $T = T^s$ toward an arbitrary coordinate R with temperature T:

$$\int_{R_d}^{R} \frac{dr}{r^2} = 4\pi\lambda \int_{T^s}^{T} \frac{dT}{\sum_{k=1}^{N} \dot{m}_k c_{p,k} (T - T^s) - \dot{Q}} \tag{16}$$

The above integration yields:

$$\sum_{k=1}^{N} \dot{m}_k c_{p,k} = \frac{4\pi\lambda}{\left(\frac{1}{R_d} - \frac{1}{R}\right)} \ln \left| \frac{\sum_{k=1}^{N} \dot{m}_k c_{p,k} (T^s - T) + \dot{Q}}{\dot{Q}} \right|. \tag{17}$$

The multi-component Spalding heat transfer number can then be defined as:

$$B_T = \frac{\sum_{k=1}^{N} \dot{m}_k c_{p,k} (T^s - T^\infty)}{\dot{Q}}, \tag{18}$$

Which allows Eq. 17 to be recast as:

$$\sum_{k=1}^{N} \dot{m}_k c_{p,k} = \frac{4\pi\lambda}{\left(\frac{1}{R_d} - \frac{1}{R}\right)} \ln|1 + B_T|. \tag{19}$$

In particular, attention is drawn here to the appearance of an absolute value operator on the RHS. As discussed in [3], this is due to the rigorous definition of the analytical integration performed on the logarithm term. This can be important for the general multi-component case since it is physically possible to have $B_T < -1$ if some species undergo condensation.

In the literature, it is also customary to define the fractional evaporation rate for each species ε_i:

$$\varepsilon_i = \frac{\dot{m}_i}{\dot{m}}. \tag{20}$$

Notice that $\sum_{k=1}^{N} \varepsilon_k = 1$ by definition. Fractional evaporation rates can then be used in Eq. 19 to isolate the global mass transfer rate:

$$\dot{m} = \frac{4\pi}{\left(\frac{1}{R_d} - \frac{1}{R}\right)} \frac{\lambda}{\sum_{k=1}^{N} \varepsilon_k c_{p,k}} \ln|1 + B_T|. \tag{21}$$

In the special case where the integration is done from the surface of the droplet toward infinity, $R \to \infty$ and Eq. 21 becomes:

$$\dot{m} = 4\pi R_d \frac{\lambda}{\sum_{k=1}^{N} \varepsilon_k c_{p,k}} \ln|1 + B_T|. \tag{22}$$

Alternatively, to account for convection effects in the gas phase, a boundary layer theory can be used with $R = R_d + \delta_T$ in Eq. 21, with δ_T being the thickness of the thermal boundary layer:

$$\dot{m} = 4\pi R_d \left[\frac{R_d + \delta_T}{\delta_T}\right] \frac{\lambda}{\sum_{k=1}^{N} \varepsilon_k c_{p,k}} \ln|1 + B_T|. \tag{23}$$

In practice, Eq. 23 is typically recast into a more usable form by using the definition of the thermal boundary layer thickness for the pure diffusive case (when the advective term, representative of the Stefan flow, is neglected) as suggested first by [30], [31]:

$$\delta_T = \frac{2R_d}{Nu_0 - 2}, \tag{24}$$

where Nu_0 is the Nusselt number computed assuming that no Stefan flow is present. In so doing, Eq. 23 becomes:

$$\dot{m} = 4\pi R_d \left[\frac{Nu_0}{2}\right] \frac{\lambda}{\sum_{k=1}^{N} \varepsilon_k c_{p,k}} \ln|1 + B_T|. \tag{25}$$

However, the energy formulation derived so far was obtained from Eq. 6, incorporating Stefan flow effects. So for consistency, the same must be done for the Nusselt number. One possible strategy is the one proposed in [23], where the thermal boundary layer thickness is corrected to add these effects through a modified Nusselt number Nu^*, defined as:

$$Nu^* = 2 + \frac{Nu_0 - 2}{F_T}, \quad F_T = (1 + B_T)^{0.7} \frac{\ln(1 + B_T)}{B_T}, \tag{26}$$

and this correction allows for the obtention of the Stefan-flow corrected version of Eq. 25:

$$\dot{m} = 4\pi R_d \left[\frac{Nu^*}{2}\right] \frac{\lambda}{\sum_{k=1}^{N} \varepsilon_k c_{p,k}} \ln|1 + B_T|. \tag{27}$$

In the particular case of a single-component droplet, by indexing the single fuel species in the gaseous phase as V for vapor and the single inert species as I, then $\sum_{k=1}^{N} \varepsilon_k c_{p,k} = \varepsilon_v c_{p,V} + \varepsilon_i c_{p,I} = c_{p,V}$, since $\varepsilon_i = 0$. Eq. 27 then degenerates to:

$$\dot{m} = 4\pi R_d \left[\frac{Nu^*}{2}\right] \frac{\lambda}{c_{p,V}} \ln|1 + B_T|, \quad B_T = \frac{\dot{m} c_{p,V}(T^s - T^\infty)}{\dot{Q}}, \tag{28}$$

As presented in the methodology of Abramzon and Sirignano [23], species and energy results are coupled through the relationship of mass and heat Spalding numbers B_M, B_T. For a single-component droplet, it is physically impossible to have $B_M < -1$ since mass fractions would need to be greater than one. Therefore, due to their coupling, it would also be impossible to have $B_T < 1$; the absolute value operator in Eq. 28 can therefore be dropped, leading to identical energy formulations between ours and the one in [23]. This way, the proposed formulation in this section is demonstrated to consistently degenerate the multi-component theory to a validated single-component one while considering the Stefan flow, enthalpy diffusion, and gas-phase convection.

To highlight the analytical impact of the enthalpy diffusion, it is useful to note that hypothesis #8 (ideal gases) can directly be made on Eq. 10, leading to:

$$\dot{m} c_p (T - T^s) + 4\pi r^2 \rho \sum_{k=1}^{N} Y_k \mathrm{v}_k^D c_{p,k} (T - T^s) - 4\pi r^2 \lambda \frac{dT}{dr} = \dot{Q}. \tag{29}$$

Now, a common strategy mentioned in the introduction is to assume that specific heats for all species in the gas phase are equal, say $\bar{c}_p$. With this assumption, it follows that $c_{p,k} = \bar{c}_p \; \forall \; k$ and also that $c_p = \sum_{k=1}^{N} Y_k c_{p,k} = \sum_{k=1}^{N} Y_k \bar{c}_p = \bar{c}_p$ such that the middle term of the LHS of Eq. 29 above can be rearranged:

$$\dot{m} \bar{c}_p (T - T^s) + \left(4\pi r^2 \rho \bar{c}_p (T - T^s)\right) \left(\sum_{k=1}^{N} Y_k \mathrm{v}_k^D\right) - 4\pi r^2 \lambda \frac{dT}{dr} = \dot{Q}. \tag{30}$$

However, from global mass conservation, it must follow that $\sum_{k=1}^{N} Y_k \mathrm{v}_k^D = 0$, canceling out the middle term of the LHS. Eq. 30 then becomes:

$$\dot{m} \bar{c}_p (T - T^s) - 4\pi r^2 \lambda \frac{dT}{dr} = \dot{Q}, \tag{31}$$

This result can be retrieved from Eq. 6, if the enthalpy diffusion term $\sum_{k=1}^{N} Y_k \mathrm{v}_k^D h_{s,k}$ is neglected, and if the equal specific heat of the gaseous mixture is expressed as $c_p = \bar{c}_p$. Therefore, the hypotheses of equal specific heats in the gaseous phase and negligible enthalpy diffusion flux are demonstrated to be equivalent whenever hypothesis #8 (ideal gases) is enforced.

Integration of Eq. 31 above follows the same steps as done for Eq. 15 and so the final result with convection effects can be rearranged as:

$$\dot{m} = 4\pi R_d \left[\frac{Nu^*}{2}\right] \frac{\lambda}{\bar{c}_p} \ln|1 + B_T|, \quad B_T = \frac{\dot{m}\bar{c}_p(T^s - T^\infty)}{\dot{Q}}. \tag{32}$$

Notice that the multi-component Spalding heat transfer number differs from the one presented in Eq. 18.

Now, when assuming equal specific heats for all species, there is an arbitrariness when choosing the value of the equal, average specific heat. This information is often opaque in most multi-component treatments in the literature. For instance, in [32], the author explicitly states that the specific heat of the fuel vapor should be used as the average specific heat for single-component droplets, as in [23]. However, no information on this is given when tackling the multi-component counterpart. In [33] it is stated that, for single-component droplets, when the Lewis number of the gaseous phase is assumed as unitary $Le = 1$, specific heats between the unique fuel vapor V and inert species I must be equal, i.e., $c_{p,V} = c_{p,I}$. This approach has been extended to a multi-component scenario for instance in [34], but no details are given on how the equal specific heat is computed; this also applies to other works of the same group [35]. In [22], even though a DCM is not used, a heat balance equation is given in terms of the specific heat of the whole gaseous mixture, c_p; in [8], no specifications are given on how their specific heat c_p is defined, even though a unitary Lewis number is also assumed. In [36], the author sums the contributions of the heat of each individual species as if they were evaporating in a single-component scenario, obtaining an expression that includes specific heats for each fuel vapor, and this by definition neglects the enthalpy diffusion. As shown in this derivation, the consistent way to incorporate enthalpy diffusion is through Eq. 25. Therefore, to the best of our knowledge, models that suggest that the specific heat in the multi-component case should include only fuel vapors, do so in analogy with the single-component case, where using $c_{p,V}$ is the reference solution.

To illustrate the two different possibilities of the average specific heat approach and to compare them with our proposed formulation, we recast all models in the following generic form:

$$\dot{m} = 4\pi R_d \left[\frac{Nu}{2}\right] \frac{\lambda}{\tilde{c}_p} \ln|1 + B_T|, \tag{33}$$

with the average specific heats $\tilde{c}_p$ and the nomenclature used for the remainder of this manuscript defined in Table A.1. This is a simple method to describe the influence of including or not enthalpy diffusion effects[1].

In particular, we note that the summation $\sum_{k=1}^{N} \varepsilon_k c_{p,k}$ for when enthalpy diffusion is incorporated takes into account all species in the gaseous phase, including inert ones. However, a common hypothesis is that there is no net dissolution of inert gas species, and this is naturally incorporated into the proposed result since $\varepsilon_k = 0$ for all inerts in

[1] In Eq. 33, we can use $Nu = 2$ for non-convective cases and $Nu = Nu^*$ as computed from Eq. 26 for instance, for convective cases.

that case. On the other hand, inert gases may still participate in the average specific heat if the $\tilde{c}_{p,\forall}$ strategy is used. As shown in the derivation process, when neglecting enthalpy diffusion, c_p may represent the whole mixture. Also, the use of fractional evaporation rates ε means that condensating species bring negative contributions to the average specific heat, which cannot be captured with both strategies that neglect enthalpy diffusion.

4. Species integration and global numerical procedure

To obtain the mass transfer rate for each species, the same procedure as in [3] is used. The diffusion velocities are computed through an equation analogous to Fick's law for the binary case, which, when assuming spherical symmetry, yields:

$$Y_i \mathrm{v}_i^D = -D_i \frac{dY_i}{dr}. \tag{34}$$

Here, the diffusion coefficient formulation for each species D_i is credited to Wilke, and can be found in the publication of Fairbanks and Wilke [13] as well as Coffee and Heimerl [37], and has also been recently used in [38] for instance. The formulation reads:

$$D_i = \frac{(1 - X_i)}{\sum\limits_{\substack{k=1 \\ k \neq i}}^{N} X_k / D_{i,k}}. \tag{35}$$

As shown in [3], the substitution of Eq. 34 in Eq. 9 followed by a second integration leads to the following result:

$$\dot{m} = 4\pi R_d \left[\frac{S\, h_k^*}{2} \right] \rho D_i \ln \left| \frac{\dot{m}_k - \dot{m} Y_k^\infty}{\dot{m}_k - \dot{m} Y_k^s} \right|. \tag{36}$$

It must be noted that to obtain the above, the product ρD_i is assumed to be constant in space. Alternatively, one can assume both transport properties ρ, D_i to be constant in space each independently; with hypothesis #9 made before for the energy, this essentially characterizes a single hypothesis of constant properties in space for the whole heat and mass transfer problem. Furthermore, to obtain the above mass transfer formalism, Soret effects (thermal diffusion impacting mass diffusion) were neglected to simplify the Stefan-Maxwell equations. However, since the proposed energy formulation does not include any explicit function from the mass transfer, it could be coupled with a more general mass transfer formulation that can incorporate Soret effects.

In [5], for instance, it is mentioned that, except when assuming equal diffusion coefficients for all species, i.e. $D_i = \bar{D}$, then the structure of Eq. 34 is such that global mass conservation is not organically preserved in general, i.e., $\sum_{k=1}^{N} Y_i \mathrm{v}_i^D \neq 0$. To circumvent this, Eqs. 36 are solved for $N-1$ species, with a last species Ω chosen to enforce global mass conservation through:

$$Y_\Omega = 1 - \sum_{\substack{k=1 \\ k \neq \Omega}}^{N} Y_k. \tag{37}$$

Then, Ω is chosen to be an inert species i.e., $\dot{m}_\Omega = 0$ such as air, and this approach is not expected to significantly impact the computation of the droplet's heat and mass transfer; the impact would mostly lie on mass fractions and, therefore, on the computations of average properties. Within this framework, Eq. 36 represents $N-1$ equations being solved for N variables: all $\dot{m}_k \; \forall \; k \neq \Omega$ and the global mass transfer rate $\dot{m}$. To close the mass transfer system, the final equation is obtained trivially:

$$\dot{m} = \sum_{k=1}^{N} \dot{m}_k. \tag{38}$$

For the numerical resolution procedure, Eq. 36 is recast in two equations to open up the absolute value operator. In this way, the mass transfer rates of each species are isolated:

$$\dot{m}_k = \dot{m} \left(\frac{Y_k^\infty - Y_k^s \exp\left[\frac{\dot{m}}{2\pi R_d S h_k^* \rho D_k}\right]}{1 - \exp\left[\frac{\dot{m}}{2\pi R_d S h_k^* \rho D_k}\right]} \right), \text{ if } \frac{\dot{m}_k - \dot{m} Y_k^\infty}{\dot{m}_k - \dot{m} Y_k^s} > 0 \tag{39a}$$

$$\dot{m}_k = \dot{m} \left(\frac{Y_k^\infty + Y_k^s \exp\left[\frac{\dot{m}}{2\pi R_d S h_k^* \rho D_k}\right]}{1 + \exp\left[\frac{\dot{m}}{2\pi R_d S h_k^* \rho D_k}\right]} \right), \text{ if } \frac{\dot{m}_k - \dot{m} Y_k^\infty}{\dot{m}_k - \dot{m} Y_k^s} < 0. \tag{39b}$$

As for implementing the energy formulation, the variable of interest is the heat transfer rate $\dot{Q}$. Eq. 27 can be then recast to isolate $\dot{Q}$ and open up the absolute value operator:

$$\dot{Q} = \frac{\dot{m} \tilde{c}_p (T^s - T^\infty)}{\exp\left[\frac{\dot{m}\tilde{c}_p}{2\pi R_d N u^* \lambda}\right] - 1}, \quad \text{if} \quad 1 + B_T > 0, \tag{40a}$$

$$\dot{Q} = -\left(\frac{\dot{m} \tilde{c}_p (T^s - T^\infty)}{\exp\left[\frac{\dot{m}\tilde{c}_p}{2\pi R_d N u^* \lambda}\right] + 1} \right), \quad \text{if} \quad 1 + B_T < 0. \tag{40b}$$

As discussed and shown in [3], care must be taken when implementing Eqs. 39 and 40 in a version that utilizes fractional evaporation rates, e.g., with $\tilde{c}_p = \sum_{k=1}^{N} \varepsilon_k c_{p,k}$ per Eq. 27. This is because there are cases where the global evaporation rate $\dot{m}$ might cross from positive to negative values (global evaporation to global condensation behavior) or vice-versa during the droplet's lifetime. This crossing of zero can create a singularity, as seen in Eq. 20, with $\dot{m} \to 0$ but with any $\dot{m}_i \nrightarrow 0$. Numerically, an overshoot is seen for the fractional evaporation rates ε_k followed by their abrupt change of sign. When using the $\tilde{c}_{p,\varepsilon}$ formulation, the handling of this sharp behavior can be avoided by solving Eqs. 40 directly with individual evaporation rates through the following set of equations:

$$\dot{Q} = \frac{\sum_{k=1}^{N} \dot{m}_k c_{p,k} (T^s - T^\infty)}{\exp\left[\frac{\sum_{k=1}^{N} \dot{m}_k c_{p,k}}{2\pi R_d N u^* \lambda}\right] - 1}, \quad \text{if} \quad 1 + B_T > 0, \tag{41a}$$

$$\dot{Q} = -\left(\frac{\sum_{k=1}^{N} \dot{m}_k c_{p,k} (T^s - T^\infty)}{\exp\left[\frac{\sum_{k=1}^{N} \dot{m}_k c_{p,k}}{2\pi R_d N u^* \lambda}\right] + 1} \right), \quad \text{if} \quad 1 + B_T < 0. \tag{41b}$$

In the following numerical investigations, infinite liquid conductivity is assumed, with the droplet's internal temperature is uniform spatially but still updated between time steps. To update this temperature, the heat transfer rate reaching the droplet $\dot{Q}_d = -\dot{Q}$ is split into sensible and latent heat:

$$\dot{Q}_d = m_d c_L \frac{dT_d}{dt} + \sum_{k=1}^{N} \dot{m}_k L_k, \tag{42}$$

where m_d is the droplet's mass, c_L the average specific heat of the liquid mixture and L_k the latent heat of vaporization of each species. Following previous hypotheses, these properties are also assumed constant during time-steps.

A vapor-liquid equilibrium (VLE) is assumed at the droplet's surface, allowing for the computation of fuel mass fractions there. This was achieved using the UNIFAC [39] activity coefficient method to incorporate non-ideal mixing effects, as in [3]. Mass fractions inside the droplet are updated between time steps from mass conservation and are also assumed to be homogeneous inside the droplet, i.e., infinite liquid mass diffusivity.

The infinite liquid thermal conductivity and mass diffusivity hypotheses are frequently employed in the literature, and so they are also applied here. Still, it must be pointed out that the energy results developed in Section 3 of this work are derived for the gas phase. Therefore, they could be coupled with different treatments for the liquid phase without additional complexities.

Finally, even though a particular emphasis is placed here on the enthalpy diffusion and the computation of the average specific heat $\tilde{c}_p$, it should be highlighted that our proposed formulation expands further than this, through the use of the absolute value operator as an extension toward more general condensation/evaporation scenarios, the consistent incorporation of convection and Stefan flow effects, and also through its coupling with a robust mass transfer counterpart validated in [3]. In this way, we highlight that this proposed novel heat and mass transfer coupled formulation is structurally different from previously mentioned approaches in the literature.

5. Results

Four different liquid mixtures are studied that can represent typical fuels or fuel additives to measure the impact of including the enthalpy diffusion. Single-droplet simulations are conducted, with droplets composed of ethanol and water (E/W), ethanol and iso-octane (E/O), acetone, ethanol, butanol, and water (A/E/B/W) and finally n-octane, n-decane, n-dodecane, n-tetradecane, and n-hexadecane (Alk), with their initial compositions listed in Table A.2.

Shared parameters to all simulations conducted in our study are the droplet's initial temperature and velocity, $T_{d,0} = 300K$ and $U_{d,0} = 0m/s$ respectively. The droplet velocity is left free and thus varies throughout its lifetime, such that $U_d \rightarrow U^\infty$ as the momentum relaxation time is reached. Four other main parameters have been varied in the simulations: the droplet's initial diameter $\mathcal{D}_0$, surrounding gas velocity U^∞,

surrounding gas temperature T^{∞}, and surrounding gas composition Y^{∞}. The numerical study swept droplets with initial diameters spanning the range $10\mu m < \mathcal{D}_0 < 40\mu m$ and surrounding gas velocity $0m/s < U^{\infty} < 30m/s$. However, for all results depicted here, the initial diameter $\mathcal{D}_0 = 20\mu m$ and the surrounding velocity $U^{\infty} = 10m/s$ are fixed, since their variation was not impactful for the analysis of enthalpy diffusion models.

Simulations are conducted with only air as the inert species, such that Ω is air in Eq. 37, and the presence of fuel vapors in the atmosphere was varied as follows. First, each droplet is exposed to a pure air atmosphere as a control case, namely $[\Omega] = 1.0$ or equivalently $Y^{\infty} = 0$ for all fuels. This control case is referred to here as "Air". For the other cases, fuel concentrations are varied in terms of the Relative Vapor Presence (RVP) parameter $0 < \phi_i^{\mathrm{RVP}} < 1$:

$$X_i^{\infty} = \phi_i^{\mathrm{RVP}} \left[\frac{p_{sat,i}(T = T_{d,0} = 300K)}{p_{atm}} \right], \tag{43}$$

which is here used to compute a molar fraction characterized by the ratio of the vapor pressure for each species at the droplet's initial temperature ($300K$) to the maximum theoretical value corresponding to the atmospheric pressure $p_{atm} = 101325Pa$. All depicted test cases are summarized in Table A.3, using the ϕ_i^{RVP} factor from Eq. 43 for each liquid composition. The remaining molar fraction at infinity is always attributed to air through Eq. 37.

A first comparison is reported between Figs. A.1 and A.2, where only the surrounding composition is changed, from E/W-Air in Fig. A.1 to E/W-RVP in Fig. A.2, following Table A.3. In both figures, enthalpy diffusion effects are not impactful, with all three models for the specific heat yielding essentially the same results in terms of mass and heat transfer rates. Still, in Fig. A.2, it is possible to see that a significant difference is present for the average specific heat $\tilde{c}_p$. This is because of local water condensation (positive mass transfer rates for water, i.e., $\dot{m}_{d,\mathrm{H_2O}} > 0$) while ethanol, the second component, exhibits a negative mass transfer. As previously mentioned, since mass fractions Y_k are always bounded between 0 and 1, fractional evaporation rates ε_k can be negative or exceed 1, a more significant difference between average specific heats $\tilde{c}_p$ can generally be expected for such cases. Still, for these low-temperature scenarios, the effect of the inclusion of enthalpy diffusion is negligible. This can be readily justified through Eq. 33, where it is seen that if the temperature difference $|T^s - T^{\infty}|$ is small, then $\ln(1 + B_T) \rightarrow B_T$, cancelling out the $\tilde{c}_p$ inside the B_T expression with the other $\tilde{c}_p$ outside of it, functionally eliminating the dependency on this average specific heat.

With this first observation in mind, it was found that in general the most critical parameter that highlights differences among strategies for handling the enthalpy diffusion was the surrounding gas temperature T^{∞}. It was observed that as the temperature increases, the impact is accentuated, especially for the $\tilde{c}_{p,\forall}$ average specific heat formulation that takes into account all gaseous species. This is directly visible when now comparing Figs. A.2 and A.3, which still depict the E/W-RVP liquid composition from Table A.3, but now at different temperatures, $T^{\infty} = 300.01K$ versus $T^{\infty} = 1800K$, respectively. It is remarkable that the strategy that neglects enthalpy diffusion by assuming equal

specific heats with only fuel contributions, $\tilde{c}_{p,F}$ in Table A.1, can predict similar results to $\tilde{c}_{p,\varepsilon}$, which incorporates enthalpy diffusion consistently, as seen in Fig. A.3. This contrasts with the $c_{p,\forall}$ formulation, which impacts the overall droplet lifetime of around 30%. Even though this impact depends only on the choice of the average specific heat, a main quantity for the energy formulation, differences in normalized heat transfer rates still appear to not be too significant, so care must be taken when analyzing these metrics.

In Figs. A.4, A.5 and A.6, results are presented for the remaining liquid compositions from Table A.3. Due to the mentioned small importance of the average specific heat for low-temperature scenarios, only results for high temperatures are depicted. For all droplet compositions, we see that neglecting enthalpy diffusion when taking inert species into account, i.e., $\tilde{c}_{p,\forall}$, tends to have a greater impact on mass transfer rates, as opposed to heat transfer rates. Again, this may reinforce the idea that heat and mass transfer are strongly coupled since the specific heat is an energy-related parameter. Also, impacts are typically manifested through an "anticipative" behavior - for example, mass tends to be released "sooner" when neglecting enthalpy diffusion with inert species taken into account in the specific heat. This may be quite impactful for spray combustion applications when trying to predict a flame structure that accounts for all participating fuel species. This behavior also leads to higher droplet lifetime predictions when consistently including enthalpy diffusion effects, which is also among the conclusions presented by Lupo and Duwig [15]. It is also possible to justify this using a simple physical analysis. As seen in Figs. A.3 or A.4 for example, the inclusion of inert species reduces the specific heat of the gaseous mixture. Since the specific heat is a measure of how much energy is necessary to raise the temperature of a mixture, this means that for a given supplied heat, more of it would be available to reach the surface of the droplet if a smaller specific heat is computed. This supplementary energy is then used to heat the droplet more quicker, leading to faster evaporation rates.

To better quantify the impact of high-temperature environments when taking inert species into account, simulations following the same cases as in Figs. A.3-A.6 were performed but with increasing surrounding gas temperature, from $T^{\infty} = 300.01K$ to $T^{\infty} = 1800K$ in increments of $\Delta T^{\infty} = 100K$. The following metric is then defined:

$$\Delta t_{evap}(\%) = \left(\frac{t_{evap}^{\tilde{c}_{p,\varepsilon}} - t_{evap}^{\tilde{c}_{p,\forall}}}{t_{evap}^{\tilde{c}_{p,\varepsilon}}} \right) * 100, \tag{44}$$

where $t_{evap}^{\tilde{c}_{p,\varepsilon}}$ is the time to evaporate when including enthalpy diffusion and $t_{evap}^{\tilde{c}_{p,\forall}}$ is the time to evaporate when neglecting enthalpy diffusion by using an average specific heat that takes inert species into account, see Table A.1. As discussed before, the initial diameter $\mathcal{D}_0 = 20\mu m$ and surrounding velocity $U^{\infty} = 10m/s$ are kept fixed, since they not play a significant role in the model comparison. Results are summarized in Fig. A.7. For all observed droplets, a relative difference of 10% is already visible starting at around $T^{\infty} = 700K$. Since realistically even higher values of T^{∞} can be expected for spray combustion applications, the use of the $c_{p,\forall}$ strategy is not recommended. It is to be noted that the same overall trend can be seen for all droplet compositions.

Still, for the cases in Figs. A.1-A.6, the strategy that neglects enthalpy diffusion with an average specific that only considers fuel species, $\tilde{c}_{p,F}$, presents a good agreement compared to our proposed approach based on a rigorous derivation. As discussed before, differences between the two strategies are expected to be bigger when fractional evaporation rates become negative, i.e., $\varepsilon_k < 0$. This happens when some species have an opposite mass transfer mechanism to the global one; for example, one species is condensating even though the droplet is globally evaporating (or vice-versa). To this merit, in Fig. A.8 it is possible to see that indeed not much difference is seen between fractional evaporation rates and normalized fuel mass fractions for the A/E/B/W droplet (same simulation as in Fig. A.5), even though fuel vapors from all species are present in the surrounding atmosphere. This motivates the search for cases where such differences may be significant.

In this optic, we now place droplets in flame-like conditions, by imposing fixed profiles for surrounding temperature, composition, and velocity following the theoretical framework described in [5] for one-dimensional premixed laminar flames. The droplet's position is tracked while it advances toward the flame. As a result, the droplet is impacted by varying conditions at infinity. Main details of this theoretical tool can be found in Appendix A. The flame used here was based on the one-step, stoichiometric combustion of ethanol, and droplets composed of an acetone / ethanol / butanol / water mixture were studied with varying initial compositions to try to map the impact of consistently including enthalpy diffusion. As seen in the Appendix, ethanol will be present as a fuel vapor initially, and then will phase out in favor of water, a combustion product. Also, for all cases with the imposed theoretical flame, the droplet's initial velocity was imposed to match the inlet velocity, i.e., $U_{d,0} = 0.5 m/s$. Coupled with the rising temperature, this dynamic is expected to stress the system and make fractional evaporation rates differ more from mass fractions. We omit results with the $c_{p,\forall}$ approach on the following figures for conciseness.

In Fig. A.9, a case using the flame-like conditions keeping the original A/E/B/W droplet composition from Table A.2 is plotted. Indeed, differences between average specific heats are visible, specifically at the beginning and at the later stages of the droplet's lifetime. Initially, a low-temperature scenario is present, such that this difference does not impact other metrics, as expected. It is seen however that mass transfer rates for ethanol and butanol start to deviate by half of the droplet's lifetime. This impact is also seen through a larger peak of normalized heat transfer rates for the $\tilde{c}_{p,F}$ approach. Fig. A.10 further expands this examination, with plots for fractional evaporation rates versus gaseous mass fractions and the droplet's inner composition. As expected for this more complex case, a significant difference between fractional evaporation rates and gaseous mass fractions is observed, especially at the first moments of evaporation. Still in Fig. A.10, the right image reveals that almost no difference is perceptible concerning the sequence and time in which species start to leave the droplet.

In Fig. A.11, results for a different droplet are now depicted. Initial mass fractions inside the droplet are $Y_{d,0,A} = 0.4$, $Y_{d,0,E} = 0.4$, $Y_{d,0,B} = 0.1$, and $Y_{d,0,A} = 0.1$ for acetone, ethanol, butanol and water, respectively. This can be regarded as a droplet dominated

by the most volatile compounds. Particular focus is given to the later stages of evaporation, where average specific heats separate sharply in different directions. This is better explained through Fig. A.12, where it is seen that the two different approaches predict completely different final compositions: the $\tilde{c}_{p,\varepsilon}$ approach predicts that the droplet will converge toward a single-component butanol droplet, whereas the $\tilde{c}_{p,F}$ approach predicts a single-component water droplet. As discussed in [3] for instance, the sequence in which species evaporate from a droplet can be a critical parameter for validating models seeking to describe biofuel mixtures. Specifically, the A/E/B/W droplet mixture was chosen to illustrate these conclusions since acetone/butanol/ethanol (ABE) blends can be a useful additive to enhance combustion characteristics, as seen in [40] and [41] for instance. Moreover, water is also included here as a fourth component due to its presence in the atmosphere.

It should be noted that these results are performed in a one-way coupling framework, such that the released vapor does not interfere with the flame dynamics. This is reasonable since a single droplet is being injected toward the flame. It is fair to assume that differences between specific heat approaches and the inclusion of the enthalpy diffusion should be even more pronounced when multiple droplets are present and droplet-flame interaction is rigorously accounted for.

6. Summary and conclusions

A general energy equation was derived in this work to describe the droplet heat transfer independently from any choice concerning the mass diffusion closure, i.e., the modeling of the diffusion velocities in a multi-component mixture. The point of departure is the general conservation equations of mass, species, and energy, and with common hypotheses enforced, a reference framework was developed. Through the proposed path of derivation, the effects of enthalpy diffusion, gas-phase convection, and Stefan flow can all be rigorously incorporated. Furthermore, the resulting model equations do not possess mathematical constructs that may complexify their numerical implementation or analytical structure. Simulations have then been systematically conducted to evaluate the incorporation of the enthalpy diffusion in droplet phase-change scenarios. For that, ambient gas and droplet initial parameters were varied to map conditions representative of spray combustion. In particular, a theoretical one-dimensional premixed flame was also used to represent a more complex scenario, where surrounding conditions may vary during the droplet's lifetime.

Throughout the derivation process, the proposed general multi-component formulation was clearly shown to degenerate into the energy results of the so-called Abramzon and Sirignano model [23], a validated single-component formulation. It is thus demonstrated that to obtain their established energy formulation, a development from conservation equations must consider not only the Stefan flow, as discussed in their original publication, but also enthalpy diffusion fluxes, which were previously not detailed. With this interpretation, it is possible to understand the underlying physics of one of the most employed modeling approaches for single-component droplets.

Moreover, the resulting formulation is proposed in a framework that can handle general

phase-change conditions, including extreme condensation scenarios where the Spalding heat transfer number may be negative, i.e., $B_T < -1$. The extension to convective environments is also done in a consistent fashion, and the final set of equations is presented in a robust structure that avoids singularities, as done previously for the mass transfer counterpart in [3].

Then, the impact of including the enthalpy diffusion fluxes was evaluated following our proposed approach against two possibilities encompassing strategies in the literature. Five parameters were varied to investigate the heat and mass transfer processes a droplet faces in a gaseous flow: the initial droplet diameter and composition and the gas temperature, velocity, and composition. The proposed configuration differs from the typical setup based on fixed droplets held in fibers; for this study, the droplet velocity is left to vary, as expected for a droplet moving inside a combustion chamber. In contrast to the previous studies presented in [3], not only binary but ternary, quaternary, and quinary mixtures are also tested, revealing no constraints for the modeling approach concerning the number or type of species. Non-ideal mixture effects were incorporated with the UNIFAC activity coefficient method.

At first, results showed that the impact of including the enthalpy diffusion is expressive for high-temperature environments, specifically when assuming an equal specific heat that considers all gaseous species ($c_{p,\forall}$). For these simpler cases, neglecting the enthalpy diffusion by means of an average specific heat that only considers fuel species, $\tilde{c}_{p,F}$, proved to be a suitable approximation. This motivated using a theoretical flame tool, first deployed in [3], to generate variable surrounding conditions during the droplet lifetime while still keeping a scope oriented toward spray combustion applications. In this more complex case, differences were spotted concerning the release order of individual species, as well as different peaks for the heat transfer rate and species' mass transfer rates. Even though this is an uncoupled theoretical tool, it highlights a sensibility that the $\tilde{c}_{p,F}$ approach may face in more severe phase-change scenarios, where mass fractions simply cannot capture the same physics as in our proposed framework.

In summary, we encourage the implementation of the proposed formulation for any gas-phase droplet phase-change treatment that shares the same fundamental hypotheses as those established for the derivation of this work. Further extensions can be done to relax some of the employed simplification hypotheses assumed here, including an extension to more general droplet shapes, as well as its coupling with other mass transfer formulations, which will be the subject of future works.

7. Acknowledgements

Support from the French Agence Nationale de la Recherche (ANR) in the MIMETYC project (grant ANR-17-CE22-0003) is acknowledged. We also acknowledge the financial support from São Paulo Research Foundation (FAPESP - grant 2021/14245-1) and the Coordenação de Aperfeiçoamento de Pessoal de Nível Superior – Brasil (CAPES) – Finance Code 001.

Appendix A. Theoretical one-dimensional flame developments

Following the developments in [5], the following equations are presented to generate an one-dimensional premixed laminar flame. First, the progress variable $0 < \Theta < 1$, which is a function of the position x, is defined as:

$$\Theta(x) = \left(1 - \frac{1}{\beta}\right) \exp\left[\frac{x}{\delta}\right], \text{ if } x < 0, \tag{A.1a}$$

$$\Theta(x) = 1 - \frac{1}{\beta} \exp\left[\frac{(1-\beta)x}{\delta}\right], \text{ if } x \geq 0, \tag{A.1b}$$

where the first rate parameter β, the second rate parameter α and the diffusional flame thickness δ are defined as:

$$\beta = \alpha\left(\frac{T_A}{T^b}\right), \tag{A.2a}$$

$$\alpha = \frac{(T^b - T^u)}{T^b}, \tag{A.2b}$$

$$\delta = \frac{D^u_{th}}{s_L}, \tag{A.2c}$$

where $T_A = E_A/R$ is the activation temperature, with E_A being the activation energy of the single-step chemical reaction and R the universal gas constant, T^u and T^b are the temperatures of the unburnt and the burnt state respectively, $D^u_{th} = \lambda^u/(\rho^u c^u_p)$ is the thermal diffusivity of the unburnt state, and s_L is the laminar flame speed.

With the progress variable, it is possible to define the temperature, velocity and mass fractions profile that the droplet will face at the far-away state:

$$T^\infty(x) = \Theta(x)(T^b - T^u) + T^u, \tag{A.3a}$$

$$U^\infty(x) = U^{inlet} + s_L\left(\frac{T^\infty(x)}{T^u}\right), \tag{A.3b}$$

$$Y^\infty_{Fuel}(x) = Y^u_{Fuel}\left(1 - \Theta(x)\right), \tag{A.3c}$$

where U^{inlet} and Y^u_{Fuel} are the pre-defined velocity and fuel mass fractions at the inlet of the laminar flame. For our case, there is only a single fuel to characterize the flame, and the combustion reaction is stoichiometric, i.e., $Y^u_{Fuel} = Y^{st}_{Fuel}$.

The progress variable equations are defined for $-\infty < x < \infty$, but for convenience the study is here limited to a finite region scaled symmetrically through the flame thickness, e.g., $-\gamma\delta < x < \gamma\delta$, with γ being an arbitrary scaling factor. The droplet's position is handled such that $x = 0$ at the start of the simulation, and so the symmetric region is shifted to only comprise positive numbers, i.e., $0 < x < 2\gamma\delta$.

For this specific study, the following parameters were used:

- $T^u = 300.01K$;
- $U^{inlet} = 0.5m/s$;

- $s_L = 0.5m/s$;
- $\gamma = 6$;
- $E_A = 30kcal/mol \rightarrow T_A \approx 15096.6K$.

The following single-step ethanol combustion reaction was used to generate the flame:

$$C_2H_5OH + 3O_2 + 11.28N_2 \rightarrow 2CO_2 + 3H_2O + 11.28N_2$$

The burnt flame temperature was computed following the methodology in [5], considering the present species in the adopted combustion reaction for ethanol. Assuming that each species has its own specific heat, the computed value is $T^b \approx 1886.4K$. The stoichiometric mass fraction for ethanol is computed as $Y^{st}_{Fuel} \approx 0.1006$, and the thermal diffusivity at the unburnt state was computed as being $D^u_{th} \approx 1.89\text{x}10^{-5}$. With that, the flame parameters are computed as $\alpha \approx 0.841$, $\beta \approx 6.73$ and $\delta \approx 3.78\text{x}10^{-5}$. In Fig. A.13, the profiles for temperature, velocity and mass fractions that the droplet face at infinity are plotted.

References

[1] S. S. Sazhin, Modelling of fuel droplet heating and evaporation: Recent results and unsolved problems, Fuel 196 (2017) 69–101. doi:10.1016/j.fuel.2017.01.048.
URL http://dx.doi.org/10.1016/j.fuel.2017.01.048

[2] C. K. Law, T. Y. Xiong, C. Wang, Alcohol droplet vaporization in humid air, International Journal of Heat and Mass Transfer 30 (1987) 1435–1443. doi:10.1016/0017-9310(87)90175-X.

[3] F. L. S. Filho, A. C. Santos, A. Vié, G. C. K. Filho, A new robust modeling strategy for multi-component droplet heat and mass transfer in general ambient conditions, International Journal of Heat and Mass Transfer 194 (2022) 123102. doi:10.1016/j.ijheatmasstransfer.2022.123102.
URL https://doi.org/10.1016/j.ijheatmasstransfer.2022.123102

[4] A. P. Pinheiro, O. Rybdylova, I. A. Zubrilin, S. S. Sazhin, F. L. S. Filho, J. M. Vedovotto, Modelling of aviation kerosene droplet heating and evaporation using complete fuel composition and surrogates, Fuel 305 (2021). doi:10.1016/j.fuel.2021.121564.

[5] T. Poinsot, D. Veynante, Theoretical and Numerical Combustion, 3rd Edition, 2012.

[6] F. A. Williams, Combustion theory: The fundamental theory of chemically reacting flow systems, second edition, 2018. doi:10.1201/9780429494055.

[7] O. S. Abianeh, C. P. Chen, A discrete multicomponent fuel evaporation model with liquid turbulence effects, International Journal of Heat and Mass Transfer 55 (2012) 6897–6907. doi:10.1016/j.ijheatmasstransfer.2012.07.003.

URL http://dx.doi.org/10.1016/j.ijheatmasstransfer.2012.07.003

[8] C. K. Law, Multicomponent droplet combustion with rapid internal mixing, Combustion and Flame 26 (1976) 219–233. doi:10.1016/0010-2180(76)90073-0.

[9] V. Ebrahimian, C. Habchi, Towards a predictive evaporation model for multi-component hydrocarbon droplets at all pressure conditions, International Journal of Heat and Mass Transfer 54 (2011) 3552–3565. doi:10.1016/j.ijheatmasstransfer.2011.03.031.
URL http://dx.doi.org/10.1016/j.ijheatmasstransfer.2011.03.031

[10] L. Zhang, S.-C. Kong, Multicomponent vaporization modeling of bio-oil and its mixtures with other fuels, Fuel 95 (2012) 471–480. doi:10.1016/j.fuel.2011.12.009.

[11] S. Tonini, G. E. Cossali, A novel formulation of multi-component drop evaporation models for spray applications, International Journal of Thermal Sciences 89 (2015) 245–253. doi:10.1016/j.ijthermalsci.2014.10.016.
URL http://dx.doi.org/10.1016/j.ijthermalsci.2014.10.016

[12] A. Blanc, Recherches sur les mobilités des ions dans les gaz, Journal de Physique Théorique et Appliquée 7 (1908). doi:10.1051/jphystap:019080070082501.

[13] D. F. Fairbanks, C. R. Wilke, Diffusion coefficients in multicomponent gas mixtures, Industrial & Engineering Chemistry 42 (1950) 471–475. doi:10.1021/ie50483a022.

[14] J. O. Hirschfelder, C. F. Curtiss, Flame propagation in explosive gas mixtures, Third Symposium (International) on Combustion, Reinhold, New York (1949) 121–127.

[15] G. Lupo, C. Duwig, A numerical study of ethanol-water droplet evaporation, Journal of Engineering for Gas Turbines and Power 140 (2018) 1–9. doi:10.1115/1.4037753.

[16] H. Grosshans, M. Griesing, M. Mönckedieck, T. Hellwig, B. Walther, S. R. Gopireddy, R. Sedelmayer, W. Pauer, H. U. Moritz, N. A. Urbanetz, E. Gutheil, Numerical and experimental study of the drying of bi-component droplets under various drying conditions, International Journal of Heat and Mass Transfer 96 (2016) 97–109. doi:10.1016/j.ijheatmasstransfer.2015.12.062.
URL http://dx.doi.org/10.1016/j.ijheatmasstransfer.2015.12.062

[17] E. I. Mahiques, S. Dederichs, C. Beck, P. Kaufmann, J. B. Kok, Coupling multicomponent droplet evaporation and tabulated chemistry combustion models

for large-eddy simulations, International Journal of Heat and Mass Transfer 104 (2017) 51–70. doi:10.1016/j.ijheatmasstransfer.2016.07.099.
URL http://dx.doi.org/10.1016/j.ijheatmasstransfer.2016.07.099

[18] S. Shen, Z. Che, T. Wang, Z. Yue, K. Sun, S. Som, A model for droplet heating and evaporation of water-in-oil emulsified fuel, Fuel 266 (2020) 116710. doi:10.1016/j.fuel.2019.116710.
URL https://doi.org/10.1016/j.fuel.2019.116710

[19] S. Sazhin, Droplets and sprays, Springer, 2014. doi:10.1007/978-1-4471-6386-2.

[20] W. A. Sirignano, Fluid Dynamics and Transport of Droplets and Sprays, second edi Edition, Cambridge University Press, 2010. doi:10.1115/1.483244.

[21] W. Long, P. Yi, M. Jia, L. Feng, J. Cui, An enhanced multi-component vaporization model for high temperature and pressure conditions, International Journal of Heat and Mass Transfer 90 (2015) 857–871. doi:10.1016/j.ijheatmasstransfer.2015.07.038.
URL http://dx.doi.org/10.1016/j.ijheatmasstransfer.2015.07.038

[22] P. Yi, W. Long, M. Jia, L. Feng, J. Tian, Development of an improved hybrid multi-component vaporization model for realistic multi-component fuels, International Journal of Heat and Mass Transfer 77 (2014) 173–184. doi:10.1016/j.ijheatmasstransfer.2014.05.008.
URL http://dx.doi.org/10.1016/j.ijheatmasstransfer.2014.05.008

[23] B. Abramzon, W. A. Sirignano, Droplet vaporization model for spray combustion calculations, Int. J. Heat Mass Transf. 32 (1989) 1605–1618. doi:10.1016/0017-9310(89)90043-4.
URL http://linkinghub.elsevier.com/retrieve/pii/0017931089900434

[24] S. Tonini, G. E. Cossali, An analytical model for the evaporation of multi-component spheroidal drops based on stefan–maxwell equations, International Journal of Thermal Sciences 171 (2022) 107223. doi:10.1016/j.ijthermalsci.2021.107223.
URL https://doi.org/10.1016/j.ijthermalsci.2021.107223

[25] G. E. Cossali, S. Tonini, Analytical solutions for modelling the evaporation of sessile drops, Applied Mathematical Modelling 114 (2023) 61–77. doi:10.1016/j.apm.2022.09.023.

[26] S. Tonini, G. E. Cossali, Modeling the evaporation of sessile drops deformed by gravity on hydrophilic and hydrophobic substrates, Physics of Fluids 35 (3 2023). doi:10.1063/5.0143575.

[27] R. B. B. W. E. S. E. N. L. D. J. Klingenberg, Introductory Transport Phenomena, Wiley, 2015.

[28] G. L. Hubbard, V. E. Denny, A. F. Mills, Droplet evaporation: Effects of transients and variable properties, Int. J. Heat Mass Transf. 18 (1975) 1003–1008. doi:10.1016/0017-9310(75)90217-3.

[29] M. C. Yuen, L. W. Chen, On drag of evaporating liquid droplets, Combustion Science and Technology 14 (1976) 147–154. doi:10.1080/00102207608547524.

[30] D. B. Spalding, The combustion of liquid fuels, Symposium (international) on combustion 4 (1953) 847–864.

[31] G. A. Godsave, Studies of the combustion of drops in a fuel spray-the burning of single drops of fuel, Symposium (International) on Combustion 4 (1953) 818–830. doi:10.1016/S0082-0784(53)80107-4.

[32] G. M. Faeth, Current status of droplet and liquid combustion, Prog. Energy Combust. Sci. 3 (1977) 191–224. doi:10.1016/0360-1285(77)90012-0.
URL http://linkinghub.elsevier.com/retrieve/pii/0360128577900120

[33] S. S. Sazhin, Advanced models of fuel droplet heating and evaporation, Progress in Energy and Combustion Science 32 (2006) 162–214. doi:10.1016/j.pecs.2005.11.001.

[34] A. Bader, P. Keller, C. Hasse, The influence of non-ideal vapor-liquid equilibrium on the evaporation of ethanol/iso-octane droplets, International Journal of Heat and Mass Transfer 64 (2013) 547–558. doi:10.1016/j.ijheatmasstransfer.2013.04.056.
URL http://dx.doi.org/10.1016/j.ijheatmasstransfer.2013.04.056

[35] P. Keller, T. Knorsch, M. Wensing, C. Hasse, Experimental and numerical analysis of iso-octane/ethanol sprays under gasoline engine conditions, International Journal of Heat and Mass Transfer 84 (2015) 497–510. doi:10.1016/j.ijheatmasstransfer.2015.01.011.
URL http://dx.doi.org/10.1016/j.ijheatmasstransfer.2015.01.011

[36] G. Brenn, L. J. Deviprasath, F. Durst, C. Fink, Evaporation of acoustically levitated multi-component liquid droplets, Int. J. Heat Mass Transf. 50 (2007) 5073–5086. doi:10.1016/j.ijheatmasstransfer.2007.07.036.

[37] T. P. Coffee, J. M. Heimerl, Transport algorithms for premixed, laminar steady-state flames, Combustion and Flame 43 (1981) 273–289. doi:10.1016/0010-2180(81)90027-4.

[38] S. Tonini, G. E. Cossali, A multi-component drop evaporation model based on analytical solution of stefan-maxwell equations, International Journal of Heat and Mass Transfer 92 (2016) 184–189. doi:10.1016/j.ijheatmasstransfer.2015.08.014.
URL http://dx.doi.org/10.1016/j.ijheatmasstransfer.2015.08.014

[39] A. Fredenslund, R. L. Jones, J. M. Prausnitz, Group-contribution estimation of activity coefficients in nonideal liquid mixtures, AIChE Journal 21 (1975) 1086–1099. doi:10.1002/aic.690210607.

[40] X. Ma, F. Zhang, K. Han, B. Yang, G. Song, Evaporation characteristics of acetone-butanol-ethanol and diesel blends droplets at high ambient temperatures, Fuel 160 (2015) 43–49. doi:10.1016/j.fuel.2015.07.079.
URL http://dx.doi.org/10.1016/j.fuel.2015.07.079

[41] X. Ma, F. Zhang, K. Han, G. Song, Numerical modeling of acetone-butanol-ethanol and diesel blends droplet evaporation process, Fuel 174 (2016) 206–215. doi:10.1016/j.fuel.2016.01.091.

Nomenclature	Definition	Enthalpy diffusion
$\tilde{c}_{p,\varepsilon}$	$\tilde{c}_p = \sum_{k=1}^{N} \varepsilon_k c_{p,k}$	Included
$\tilde{c}_{p,\forall}$	$\tilde{c}_p = \sum_{k=1}^{N} Y_k c_{p,k}$	Neglected
$\tilde{c}_{p,F}$	$\tilde{c}_p = \frac{\sum_{j\in\text{vapors}}^{N} Y_j c_{p,j}}{\sum_{j\in\text{vapors}}^{N} Y_j}$	Neglected

Table A.1: Average specific heats used in Eq. 33, allowing for different strategies to incorporate or not enthalpy diffusion effects.

Droplet	Initial composition (mass fractions)
E/W	$[C_2H_5OH] = 0.95$, $[H_2O] = 0.05$
E/O	$[C_2H_5OH] = 0.2$, $[C_8H_{18}] = 0.8$
A/E/B/W	$[C_3COCH_3] = 0.3$, $[C_2H_5OH] = 0.1$, $[C_4H_9OH] = 0.55$, $[H_2O] = 0.05$
Alk	$[C_8H_{18}] = 0.05$, $[C_{10}H_{22}] = 0.15$, $[C_{12}H_{26}] = 0.4$, $[C_{14}H_{30}] = 0.25$, $[C_{16}H_{34}] = 0.15$

Table A.2: Initial droplet compositions in mass fractions used in the numerical investigations of this section. "E/W" refers to ethanol/water, "E/O" to ethanol/iso-octane, "A/E/B/W" to acetone/ethanol/butanol/water, and "Alk" to n-octane/n-decane/n-dodecane/n-tetradecane/n-hexadecane.

Denomination	Surrounding gas composition
E/W-Air	$\phi^{\mathrm{RVP}}_{C_2H_5OH} = 0$, $\phi^{\mathrm{RVP}}_{H_2O} = 0$
E/W-RVP	$\phi^{\mathrm{RVP}}_{C_2H_5OH} = 0$, $\phi^{\mathrm{RVP}}_{H_2O} = 0.90$
E/O	$\phi^{\mathrm{RVP}}_{C_2H_5OH} = 0.1$, $\phi^{\mathrm{RVP}}_{C_8H_{18}} = 0.3$
A/E/B/W	$\phi^{\mathrm{RVP}}_{C_3COCH_3} = 0.1$, $\phi^{\mathrm{RVP}}_{C_2H_5OH} = 0.05$ $\phi^{\mathrm{RVP}}_{C_4H_9OH} = 0.25$, $\phi^{\mathrm{RVP}}_{H_2O} = 0.6$
Alk	$\phi^{\mathrm{RVP}}_{C_8H_{18}} = 0.1$, $\phi^{\mathrm{RVP}}_{C_{10}H_{22}} = 0.1$, $\phi^{\mathrm{RVP}}_{C_{12}H_{26}} = 0.4$, $\phi^{\mathrm{RVP}}_{C_{14}H_{30}} = 0.3$, $\phi^{\mathrm{RVP}}_{C_{16}H_{34}} = 0.2$

Table A.3: Surrounding gas compositions used in the numerical investigations of this section. In the first column, denominations are presented for respective droplets of Table A.2, with "E/W" referring to ethanol/water, "E/O" to ethanol/iso-octane, "A/E/B/W" to acetone/ethanol/butanol/water and "Alk" to n-octane/n-decane/n-dodecane/n-tetradecane/n-hexadecane. The relative vapor presence parameter ϕ_i^{RVP} is used in Eq. 43 to obtain molar fractions.

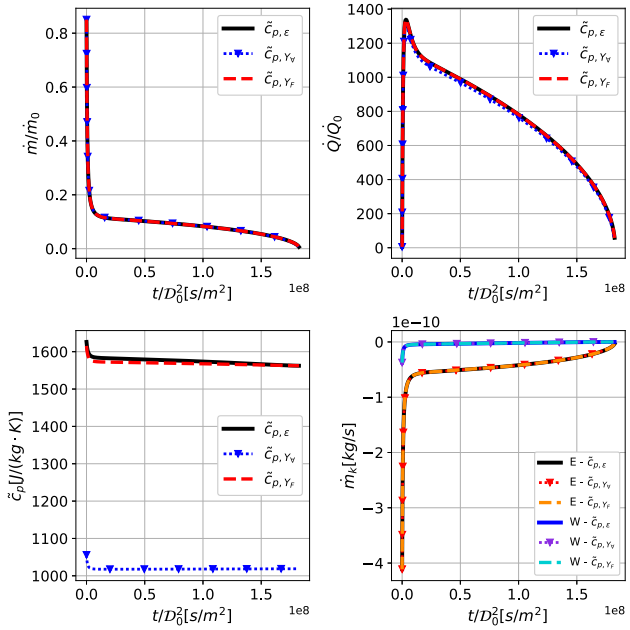

Figure A.1: Ethanol/water (E/W) droplet with $\mathcal{D}_0 = 20\mu m$, $T_{d,0} = 300K$, $T^{\infty} = 300.01$, $U_{d,0} = 0m/s$, and $U^{\infty} = 10m/s$. The surrounding gas composition is "E/W-Air" from Table A.3. Results are displayed for the non-dimensional global mass transfer rate $\dot{m}/\dot{m}_0$, non-dimensional heat transfer rate $\dot{Q}/\dot{Q}_0$, average specific heat $\tilde{c}_p$ and individual mass transfer rates $\dot{m}_k$ for each species, versus a reduced time $t/\mathcal{D}_0^2$.

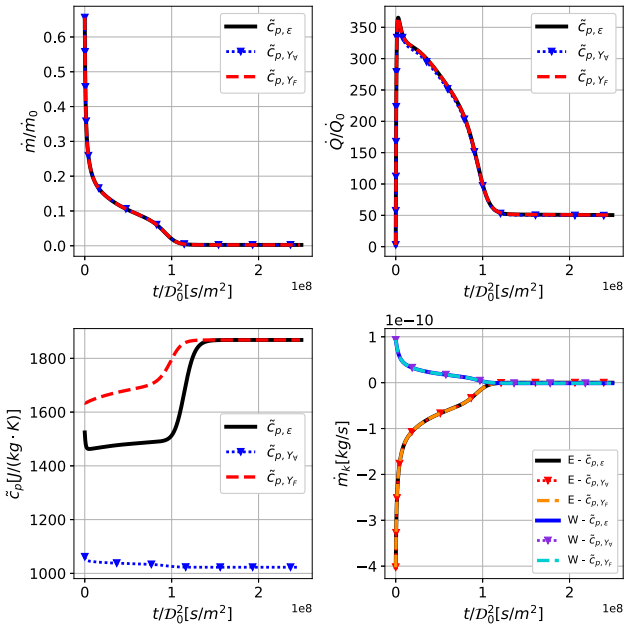

Figure A.2: Ethanol/water (E/W) droplet with $\mathcal{D}_0 = 20\mu m$, $T_{d,0} = 300K$, $T^\infty = 300.01$, $U_{d,0} = 0m/s$, and $U^\infty = 10m/s$. The surrounding gas composition is "E/W-RVP" from Table A.3. Results are displayed for the non-dimensional global mass transfer rate $\dot{m}/\dot{m}_0$, non-dimensional heat transfer rate $\dot{Q}/\dot{Q}_0$, average specific heat $\tilde{c}_p$ and individual mass transfer rates $\dot{m}_k$ for each species, versus a reduced time $t/\mathcal{D}_0^2$.

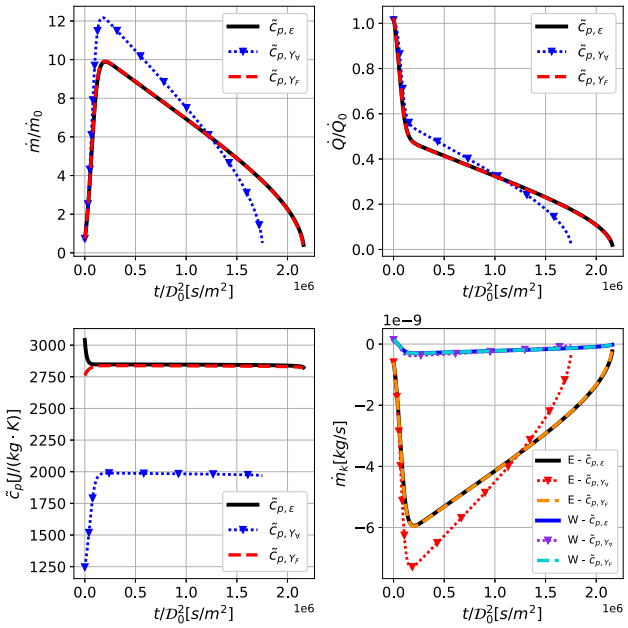

Figure A.3: Ethanol/water (E/W) droplet with $\mathcal{D}_0 = 20\mu m$, $T_{d,0} = 300K$, $T^\infty = 1800$, $U_{d,0} = 0m/s$ and $U^\infty = 10m/s$. The surrounding gas composition is "E/W-RVP" from Table A.3. Results are displayed for the non-dimensional global mass transfer rate $\dot{m}/\dot{m}_0$, non-dimensional heat transfer rate $\dot{Q}/\dot{Q}_0$, average specific heat $\tilde{c}_p$ and individual mass transfer rates $\dot{m}_k$ for each species, versus a reduced time $t/\mathcal{D}_0^2$.

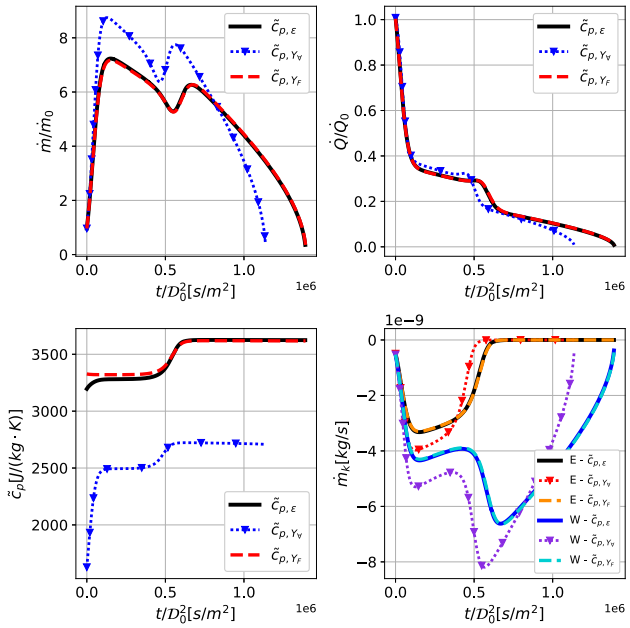

Figure A.4: Ethanol/iso-octane (E/O) droplet with $\mathcal{D}_0 = 20\mu m$, $T_{d,0} = 300K$, $T^\infty = 1800$, $U_{d,0} = 0m/s$ and $U^\infty = 10m/s$. The surrounding gas composition is "E/O" from Table A.3. Results are displayed for the non-dimensional global mass transfer rate $\dot{m}/\dot{m}_0$, non-dimensional heat transfer rate $\dot{Q}/\dot{Q}_0$, average specific heat $\tilde{c}_p$ and individual mass transfer rates $\dot{m}_k$ for each species, versus a reduced time $t/\mathcal{D}_0^2$.

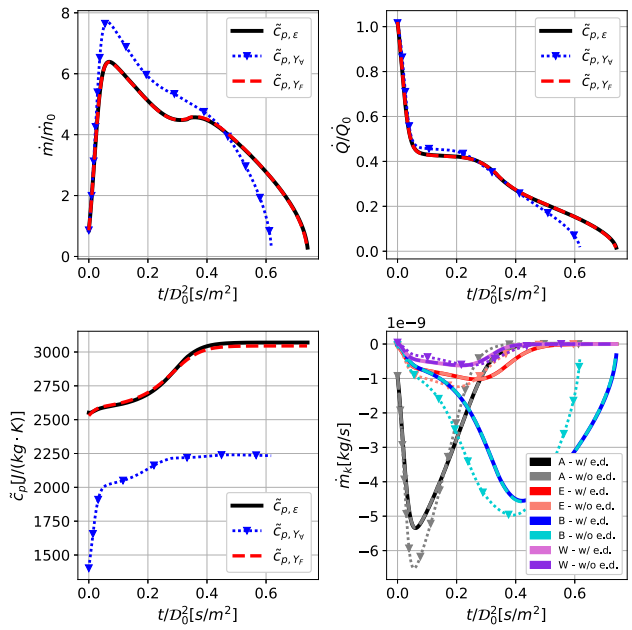

Figure A.5: Acetone/ethanol/butanol/water (A/E/B/W) droplet with $\mathcal{D}_0 = 20\mu m$, $T_{d,0} = 300K$, $T^\infty = 1800$, $U_{d,0} = 0m/s$ and $U^\infty = 10m/s$ and surrounding gas composition from Table A.3. Results are displayed for the non-dimensional global mass transfer rate $\dot{m}/\dot{m}_0$, non-dimensional heat transfer rate $\dot{Q}/\dot{Q}_0$, average specific heat $\tilde{c}_p$ and individual mass transfer rates $\dot{m}_k$ for each species, versus a reduced time $t/\mathcal{D}_0^2$. In the bottom right image, both approaches that neglect enthalpy diffusion are depicted with the same color for clarity.

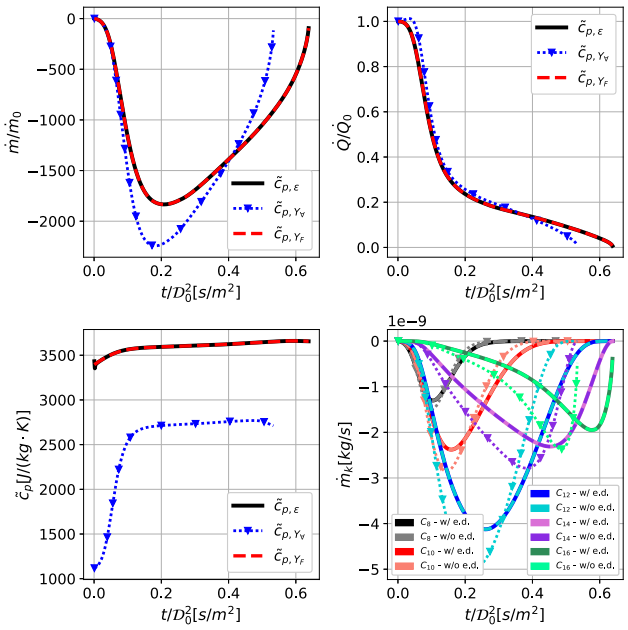

Figure A.6: N-octane/n-decane/n-dodecane/n-tetradecane/n-hexadecane (Alk) droplet with $\mathcal{D}_0 = 20\mu m$, $T_{d,0} = 300K$, $U_{d,0} = 0m/s$ and $T^\infty = 1800$, $U^\infty = 10m/s$ and surrounding gas composition from Table A.3. Results are displayed for the non-dimensional global mass transfer rate $\dot{m}/\dot{m}_0$, non-dimensional heat transfer rate $\dot{Q}/\dot{Q}_0$, average specific heat $\tilde{c}_p$ and individual mass transfer rates $\dot{m}_k$ for each species, versus a reduced time $t/\mathcal{D}_0^2$. In the bottom right image, both approaches that neglect enthalpy diffusion are depicted with the same color for clarity.

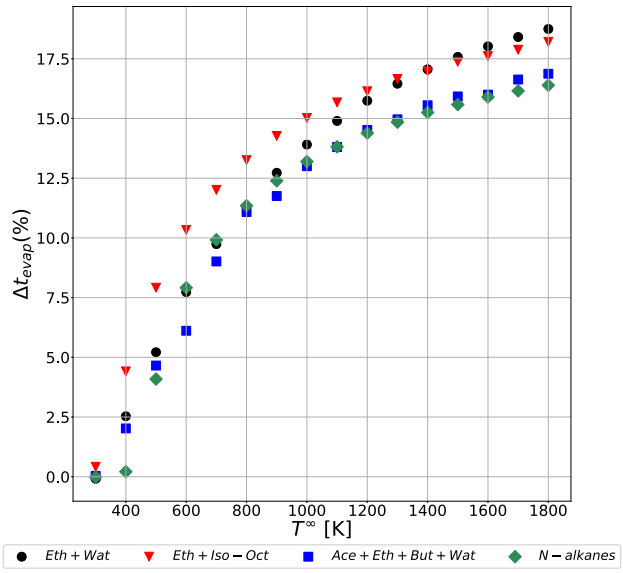

Figure A.7: Normalized evaporation time difference as described by Eq. 44 for simulations with $\mathcal{D}_0 = 20\mu m$, $T_{d,0} = 300K$, $U_{d,0} = 0m/s$ and $U^{\infty} = 10m/s$. The surrounding gas composition for the "E/W" droplet is "E/W-RVP" from Table A.3. Surrounding gas temperature is varied from $T^{\infty} = 300.01K$ to $T^{\infty} = 1800K$ in increments of $\Delta T^{\infty} = 100K$.

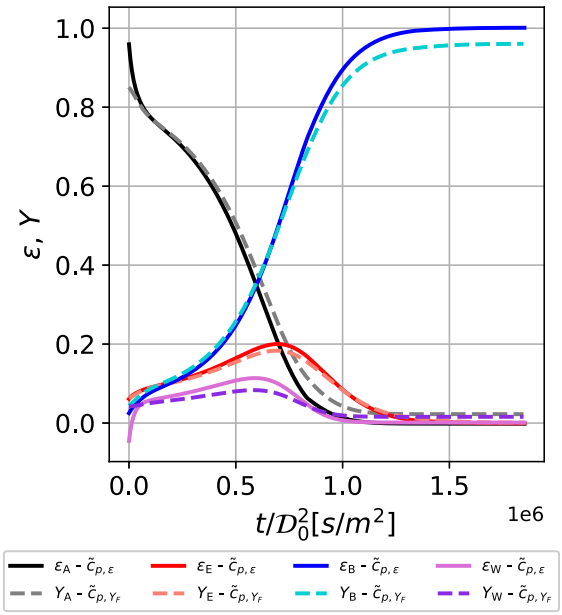

Figure A.8: Acetone/ethanol/butanol/water (A/E/B/W) droplet with $\mathcal{D}_0 = 20\mu m$, $T_{d,0} = 300K$, $T^\infty = 1800$, $U_{d,0} = 0m/s$ and $U^\infty = 10m/s$ and surrounding gas composition from Table A.3 (same case as Fig. A.5). Results are displayed for the fractional evaporation rates or mass fractions, for models $\tilde{c}_{p,\varepsilon}$ and $\tilde{c}_{p,F}$ respectively as defined in Table A.1, versus a reduced time $t/\mathcal{D}_0^2$.

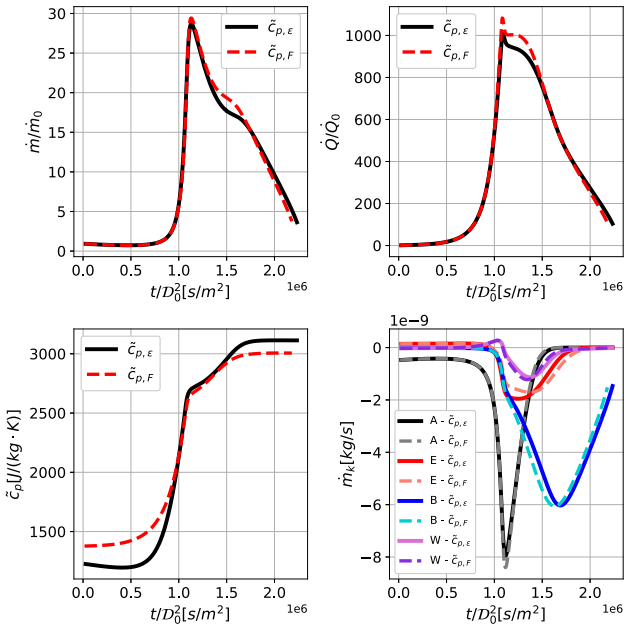

Figure A.9: Acetone/ethanol/butanol/water droplet with the A/E/B/W composition as in Table A.2, $\mathcal{D}_0 = 20\mu m$, $T_{d,0} = 300K$ and $U_{d,0} = 0.5m/s$. Surrounding conditions vary following a theoretical flame detailed in Appendix A. Results are displayed for the non-dimensional global mass transfer rate $\dot{m}/\dot{m}_0$, non-dimensional heat transfer rate $\dot{Q}/\dot{Q}_0$, average specific heat $\tilde{c}_p$ and individual mass transfer rates $\dot{m}_k$ for each species, versus a reduced time $t/\mathcal{D}_0^2$.

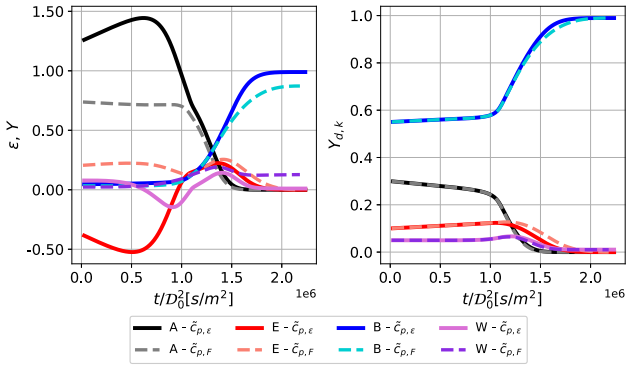

Figure A.10: Acetone/ethanol/butanol/water droplet with the A/E/B/W composition as in Table A.2, $\mathcal{D}_0 = 20\mu m$, $T_{d,0} = 300K$ and $U_{d,0} = 0.5m/s$. Surrounding conditions vary following a theoretical flame detailed in Appendix A. Results are displayed at the left for the fractional evaporation rates or gaseous mass fractions and at the right for mass fractions of each species inside the droplet, versus a reduced time $t/\mathcal{D}_0^2$.

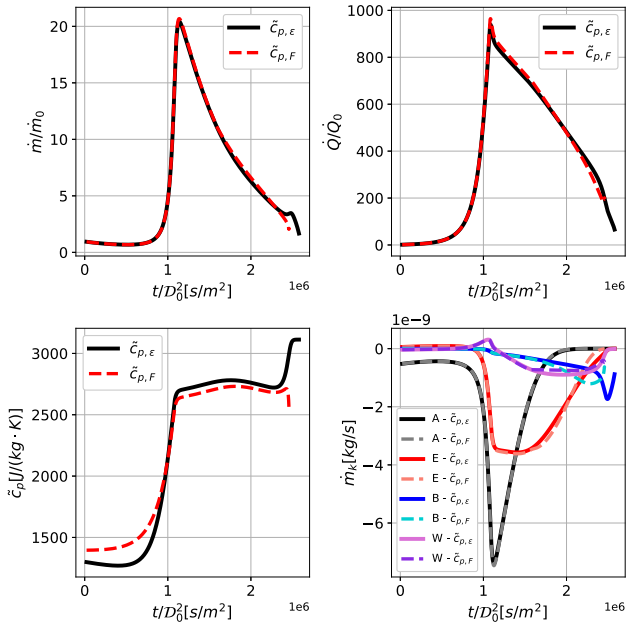

Figure A.11: Acetone/ethanol/butanol/water droplet with initial composition $Y_{d,0,A} = 0.4$, $Y_{d,0,E} = 0.4$, $Y_{d,0,B} = 0.1$, $Y_{d,0,A} = 0.1$, and $\mathcal{D}_0 = 20\mu m$, $T_{d,0} = 300K$ and $U_{d,0} = 0.5m/s$. Surrounding conditions vary following a theoretical flame detailed in Appendix A. Results are displayed for the non-dimensional global mass transfer rate $\dot{m}/\dot{m}_0$, non-dimensional heat transfer rate $\dot{Q}/\dot{Q}_0$, average specific heat $\tilde{c}_p$ and individual mass transfer rates $\dot{m}_k$ for each species, versus a reduced time $t/\mathcal{D}_0^2$.

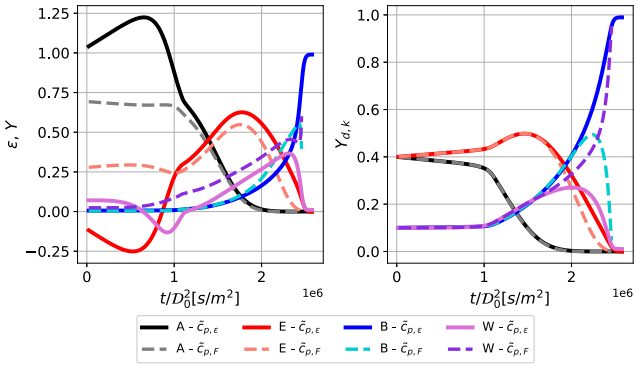

Figure A.12: Acetone/ethanol/butanol/water droplet with initial composition $Y_{d,0,A} = 0.4$, $Y_{d,0,E} = 0.4$, $Y_{d,0,B} = 0.1$, $Y_{d,0,A} = 0.1$, and $\mathcal{D}_0 = 20\mu m$, $T_{d,0} = 300K$ and $U_{d,0} = 0.5m/s$. Surrounding conditions vary following a theoretical flame detailed in Appendix A. Results are displayed at the left for the fractional evaporation rates or gaseous mass fractions and at the right for mass fractions of each species inside the droplet, versus a reduced time $t/\mathcal{D}_0^2$.

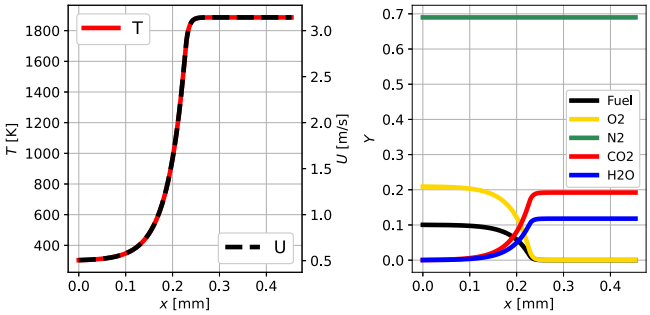

Figure A.13: At the left, temperature (T) and velocity (U) profiles and at the right, mass fraction (Y) profiles generated using parameters described in this appendix for a single-step, one-dimensional premixed ethanol laminar flame.

Nomenclature

B_M	Spalding mass transfer number
B_T	Spalding heat transfer number
c_p	Gaseous specific heat at constant pressure for the whole gaseous mixture ($J/(kg \cdot K)$)
$\bar{c}_p$	Gaseous specific heat at constant pressure when the assumption of equal specific heat for all species is made ($J/(kg \cdot K)$)
$\tilde{c}_p$	Gaseous specific heat at constant pressure used to compare different models, per Eq. 33 ($J/(kg \cdot K)$)
c_L	Average specific heat for the liquid mixture inside the droplet ($J/(kg \cdot K)$)
$c_{p,I}$	Gaseous specific heat at constant pressure for the single inert species when considering a single-component droplet ($J/(kg \cdot K)$)
$c_{p,k}$	Gaseous specific heat at constant pressure for species k ($J/(kg \cdot K)$)
$c_{p,V}$	Gaseous specific heat at constant pressure for the single fuel vapor species when considering a single-component droplet ($J/(kg \cdot K)$)
$\mathcal{D}_0$	Droplet initial diameter (m)
D_k	Average multi-component diffusion coefficient between species k and the remainder of the multi-component mixture (m^2/s)
$D_{k,j}$	Binary diffusion coefficient between species k and j in a binary mixture (m^2/s)
$\tilde{D}_{k,j}$	Binary diffusion coefficient between species k and j in a multi-component mixture (m^2/s)
$D^T_{k,j}$	Thermal diffusion coefficient between species k and j ($kg/(m \cdot s)$)
$\mathbf{f}_k$	Volumetric forces field on species k (N)
h_s	Sensible enthalpy (J/kg)
L_k	Latent heat of vaporization for species k (J/kg)
m_d	Droplet mass (kg)
$\dot{m}$	Gaseous mass transfer rate $\dot{m}_d = -\dot{m}$ (kg/s)
$\dot{m}_k$	Mass transfer rate of species k (kg/s)
Nu_0	Nusselt number in the absence of Stefan flow effects
Nu^*	Nusselt number with Stefan flow effects
$\mathbf{p}$	Pressure field (Pa)
$\mathbf{q}_R$	Radiative flux (W/m^2)
$\dot{Q}$	Heat transfer rate (J/s)
$\dot{Q}_d$	Heat transfer rate from the droplet's perspective, $\dot{Q}_d = -\dot{Q}$ (J/s)
r	Radial coordinate
R	Universal gas constant ($J/(mol \cdot K)$)
R_d	Droplet instantaneous radius (m)
Sh^*	Sherwood number with Stefan flow effects
t	Time (s)
t_{evap}	Droplet lifetime (s)
T	Temperature (K)
$T_{d,0}$	Droplet initial temperature (K)
T^s	Temperature at the surface of the droplet (K)
T^∞	Temperature far away from the droplet (K)
$\mathbf{u}$	Velocity field (m/s)
$U_{d,0}$	Droplet initial velocity (m/s)
U^∞	Surrounding field velocity (m/s)
$\mathbf{v}^D_k$	Mass diffusion velocity of species k (m/s)
$\mathbf{v}^m_k$	Average molecular velocity of species k (m/s)
W_k	Molar weight of species k (kg/mol)
X_k	Molar fraction of species k
Y_k	Mass fraction of species k
δ_T	Thermal boundary layer thickness (m)
ε_k	Fractional evaporation rate of species k, $\varepsilon_k = \dot{m}_k/\dot{m}$
λ	Thermal conductivity ($W/(m \cdot K)$)
ρ	Density (kg/m^3)
$\boldsymbol{\tau}$	Viscous tensor (Pa)
ϕ^{RVP}_k	Relative vapor presence parameter for species k, as per Eq. 43
$\dot{\omega}_c$	Chemical reactions energy source term (W/m^3)
$\dot{\omega}_k$	Chemical reaction source term,